The Vorticity Budget of Synoptic-Scale Wave Disturbances in the Tropical Western Pacific[1]

RICHARD J. REED AND RICHARD H. JOHNSON

Dept. of Atmospheric Sciences, University of Washington, Seattle 98195

(Manuscript received 19 March 1974, in revised form 3 June 1974)

ABSTRACT

Composite fields of the large-scale variables determined from three months of observations at a triangular array of stations are used to determine the vorticity budget of easterly wave disturbances in the tropical western Pacific. The measurements reveal substantial imbalances which are largest in the disturbed or convectively active region of the waves. In this region there exists an apparent vorticity sink for the large-scale motions in the lower half of the troposphere and an apparent source in a relatively thin layer of the upper troposphere.

Cumulus modelling assumptions are employed to estimate vertical cloud mass flux and vertical profiles of cloud vorticity. It is concluded that the low-level sink and upper-level source can be attributed to the removal of vorticity-rich air from the lower layers and its deposition aloft by deep convection.

1. Introduction

In an earlier paper Reed and Recker (1971) used three months of data from stations in the tropical western Pacific to determine the structure and properties of the westward-moving synoptic-scale disturbances which traverse the region during the wet season (July–September). Composite fields of the basic meteorological variables were obtained by assigning each observation to one of eight specified sectors of the associated wave disturbance and forming averages. Mass, moisture and heat budgets for the various wave sectors were also obtained.

The primary purpose of the present paper is to employ the same data set and compositing technique to determine the vorticity budget of the wave disturbance. This budget is of particular interest in view of the finding of Riehl and Pearce (1968) and of Williams (1970) that sizeable imbalances exist when it is evaluated from large-scale variables alone. Their result, if correct, implies that convective-scale motions exert a significant effect on the vorticity budget and suggests that in modelling tropical disturbances attention must be given to parameterizing convective effects in the momentum equation as well as in the thermodynamic energy and water mass continuity equations.

A second objective of the present paper is to deduce from the same data set properties of the convective ensembles embedded within the waves, in particular the vertical cloud mass flux and in-cloud vorticity. A combination of the observed large-scale vorticity changes and a convective ensemble model, patterned after that of Yanai *et al.* (1973), is employed in deriving the properties. Previous estimates of the cloud mass flux, based on large-scale heat and moisture budgets, have been made by Yanai *et al.*, Ogura and Cho (1973) and Reed and Johnson (1974).

2. Equations and method of solution

We start with the vorticity equation written in flux form with the twisting terms neglected:

$$\frac{\partial \eta}{\partial t}+\nabla\cdot\eta\mathbf{V}+\frac{\partial}{\partial p}\eta\omega=\eta\frac{\partial \omega}{\partial p},$$

or

$$\frac{\partial \eta}{\partial t}+\nabla\cdot\eta\mathbf{V}+\omega\frac{\partial \eta}{\partial p}=0, \tag{1}$$

where η is the absolute vorticity (the sum of the relative vorticity ζ and the Coriolis parameter f), $\mathbf{V}$ the horizontal velocity, ω the vertical p-velocity, t time, and p pressure. Unless otherwise specified, vorticity will hereafter refer to the absolute vorticity.

Next, we define synoptic-scale variables by averaging (1) over an area large enough to include numerous convective elements but small enough to resolve the large-scale fields. An overbar is used to denote the average so defined and a prime to denote deviations therefrom. In performing the averaging, we assume that deviations of vorticity and horizontal velocity from their respective mean values are uncorrelated, that is, that the hori-

[1] Contribution No. 310, Department of Atmospheric Sciences, University of Washington.

zontal eddy flux of vorticity is negligible. Eq. (1) then takes the form

$$Z\equiv\frac{\partial\bar{\eta}}{\partial t}+\mathbf{V}\cdot\nabla\bar{\eta}+\bar{\omega}\frac{\partial\bar{\eta}}{\partial p}+\bar{\eta}\nabla\cdot\mathbf{V}=-\overline{\omega'\left(\frac{\partial\eta}{\partial p}\right)'}. \tag{2}$$

In analogy to Yanai's definitions of an apparent heat source and an apparent moisture sink, we refer to the quantity Z as the apparent vorticity source. An increase in this quantity following the three-dimensional mean motion signifies that the large-scale vorticity is being increased by convective-scale processes. Had the twisting effect been included in (1) the following additional terms would have appeared:

$$\mathbf{k}\cdot\nabla\bar{\omega}\times\frac{\partial\bar{\mathbf{V}}}{\partial p}+\mathbf{k}\cdot\overline{\nabla\omega'\times\frac{\partial\mathbf{V}'}{\partial p}},$$

where $\mathbf{k}$ is the unit vector in the vertical. The first of these terms was found to be negligible when evaluated from the data described in Section 3. It is more difficult to justify the neglect of the second term. In this respect we merely note that its neglect is consistent with the simple cloud model to be employed in which the vertical velocity is assumed to be uniform over a cross-sectional area of the cumulus. Introducing this effect would complicate the problem in ways that do not seem warranted in a first attempt at explaining the vorticity budget.

The area-mean values of η and ω may be expressed as

$$\left.\begin{aligned}\bar{\eta}&=\sigma\eta_c+(1-\sigma)\tilde{\eta}\\ \bar{\omega}&=\sigma\omega_c+(1-\sigma)\tilde{\omega}\end{aligned}\right\}, \tag{3}$$

where σ is the fractional area occupied by active cumulus convection. The subscript c indicates the value of the quantity in the convective updraft and the tilde that in the environment. With these definitions, it can be shown, following Yanai *et al.*, that

$$\overline{\omega'\left(\frac{\partial\eta}{\partial p}\right)'}\approx\sigma\omega_c\frac{\partial}{\partial p}(\eta_c-\tilde{\eta})=-M_c\frac{\partial}{\partial p}(\eta_c-\tilde{\eta}). \tag{4}$$

The quantity $M_c=-\sigma\omega_c$ represents the convective mass flux per unit area measured in pressure units. It differs from the true mass flux by a factor of g, the acceleration of gravity.

Substitution of (4) in (2) yields

$$Z=M_c\frac{\partial}{\partial p}(\eta_c-\tilde{\eta}). \tag{5}$$

Since M_c is inherently positive, it follows from (5) that an apparent vorticity source will exist where there is an excess vorticity in the clouds and this excess increases with increasing pressure (or decreases with increasing height). Correspondingly, an apparent vorticity sink occurs where the excess vorticity increases with height.

Continuing to follow the approach of Yanai *et al.*, we next write the equation of balance for vorticity between the cloud mass and the environment assuming that the convective activity is in statistical equilibrium with the large-scale motion. Thus,

$$\hat{\eta}\frac{\partial M_c}{\partial p}-\frac{\partial}{\partial p}(M_c\eta_c)+\eta_c\frac{\partial M_c}{\partial p}=0, \tag{6}$$

or

$$\hat{\eta}\frac{\partial M_c}{\partial p}-M_c\frac{\partial\eta_c}{\partial p}=0, \tag{7}$$

where, following the notation of Holton (private communication),

$$\hat{\eta}=\begin{cases}\eta_c, & \text{for } \dfrac{\partial M_c}{\partial p}>0 \quad \text{(detrainment)}\\[2ex] \tilde{\eta}, & \text{for } \dfrac{\partial M_c}{\partial p}<0 \quad \text{(entrainment).}\end{cases} \tag{8}$$

In (6), as previously, the twisting terms are neglected. The sole mechanism for generating vorticity is assumed to be the effect of horizontal convergence, as expressed by the final term in the equation.

Separate equations for the apparent vorticity source in the entrainment and detrainment regions of the convective towers are obtained from substitution of (7) in (5) with use of the relations in (8). Thus,

$$Z=\tilde{\eta}\frac{\partial M_c}{\partial p}-M_c\frac{\partial\tilde{\eta}}{\partial p} \tag{9}$$

for the entrainment region, and

$$Z=\eta_c\frac{\partial M_c}{\partial p}-M_c\frac{\partial\tilde{\eta}}{\partial p} \tag{10}$$

for the detrainment region.

But in the detrainment region (7) may be integrated to give

$$\eta_c=kM_c, \tag{11}$$

where $k=(\eta_c)_0/(M_c)_0$, the subscript referring to known boundary values. Thus, Eq. (10) may be rewritten

$$Z=M_c\left(k\frac{\partial M_c}{\partial p}-\frac{\partial\tilde{\eta}}{\partial p}\right). \tag{12}$$

Given the observed values of Z (the apparent vorticity source) and the environmental vorticity $\tilde{\eta}$, it is possible to solve (9) and (12) for the cloud mass flux M_c, and (7) and (11) for the cloud vorticity η_c. It is assumed that the environmental vorticity $\tilde{\eta}$ is represented with sufficient accuracy by the mean vorticity $\bar{\eta}$,

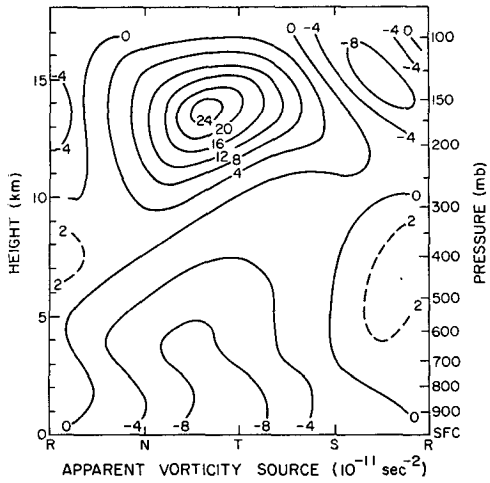

FIG. 1. Composite diagram of the apparent vorticity source. The letters R, N, T and S refer to the ridge, north wind, trough and south wind regions, respectively, of the wave disturbance.

measured from the data. This assumption is valid provided the cloud vorticity does not exceed the environmental vorticity by more than an order of magnitude. The steps in the solution are as follows:

(i). Assume a trial value of M_c at cloud base (950 mb).

(ii). Integrate (9) upward until M_c attains a maximum.

(iii). Compute η_c at the cloud base from a boundary layer vorticity balance equation analogous to the boundary layer heat and moisture balance equations employed by Yanai *et al.* (In the final results to be presented in Section 5, this method was abandoned, for reasons which will be explained later, and an assumed value of η_c was used.)

(iv). Integrate (7) vertically with use of the mass flux distribution determined in step (ii) to obtain η_c from cloud base to the level of maximum mass flux.

(v). Integrate (12) vertically from the level of maximum flux to the level where $M_c=0$. The constant k is known since M_c and η_c are already determined at the level of maximum flux.

(vi). If $M_c=0$ in the vicinity of 100 mb, where the convective activity is likely to be small, consider the solution to be satisfactory. If not, assume a new trial value of M_c at cloud base and repeat the procedure until the required condition at 100 mb is met.

(vii). Finally use (11) to obtain η_c in the detrainment layer.

In the foregoing scheme no account is taken of the possible existence of different cloud types or sizes, as in the study of Yanai *et al.* When different cloud types are present, entrainment and detrainment can occur simultaneously at the same level, and $\partial M_c/\partial p$ does not represent uniquely either entrainment or detrainment. In the simplified treatment used here only entrainment is assumed to exist where $\partial M_c/\partial p$ is negative and only detrainment where it is positive [see Eq. (8)]. It is recognized that the assumption of a single cloud type is a serious weakness of the present treatment. Attempts are being made to extend the model so as to include multiple types. Meanwhile it is felt that the results obtained from the simpler model are of sufficient interest to warrant presentation.

3. Data and measurements

The data used in this study were the same as employed in the study of Reed and Recker (1971). They consist of twice-daily soundings during the three-month period July–September, 1967, for a triangular array of stations—Kwajalein, Eniwetok and Ponape—in the Marshall Island area. Average meridional wind components, vorticities, divergences and vertical p-velocities were determined at 50-mb intervals from the surface to 100 mb in eight different sectors of the wave disturbances that passed through the array. These quantities allow all terms in the vorticity equation (2) to be measured except the horizontal advection term which contains vorticity gradients. Since the vorticity was measured only for the above-mentioned triangle of stations, an assumption is required to evaluate the gradients and hence the advection. The assumption made is that this term can be approximated by taking the sum of [the long-term (3 month) mean zonal wind component U, multiplied by the local time derivative of vorticity converted to an east-west space derivative on the basis of the average zonal wave speed c] and [the synoptic-scale, fluctuating meridional wind multiplied by the long-term mean north-south vorticity gradient]. Use was made of climatic data for the region (Wiederanders, 1961) in determining the mean gradient. Thus, according to the above assumption,

$$\bar{\mathbf{V}}\cdot\nabla\bar{\eta}=-\left[\frac{U}{c}\frac{\partial\bar{\eta}}{\partial t}+v\left(\frac{\partial^2 U}{\partial y^2}-\beta\right)\right], \qquad (13)$$

where $\beta\equiv\partial f/\partial y$, the variation of the Coriolis parameter in the y (north-south) direction. This equation should yield a sufficiently accurate measure of the advection provided the waves are in an approximately steady state as they pass through the network.

4. Results: Vorticity budget

The vorticity budget was determined for eight regions within the composite wave; namely, the regions about the trough and ridge axes, the regions about the inflection points, and the four intermediate regions. Shown in Table 1 are the results of calculations for the region of the wave trough. It is seen that the divergence or vorticity production term is the dominant one in the budget. The sum of the remaining terms, which expresses the individual change of absolute vorticity

following the three-dimensional motion, is generally much smaller. Consequently, a negative residual or apparent vorticity sink is obtained in the convergent region of the lower troposphere and a positive residual or apparent vorticity source in the upper divergent region. This result confirms Pearce's finding that the residual vorticity change is in the sense to reduce the magnitude of the vorticity in both the lower and upper troposphere.

The field of Z, the apparent vorticity source for the whole wave, is depicted in Fig. 1. Largest magnitudes occur near and somewhat ahead (west) of the wave trough position, denoted by the letter T. This is the region of heaviest rainfall and presumably the region of most intense convective activity.

It is of interest to compare the results of the foregoing computations with those of Williams (1970). For this purpose we assume that the trough and ridge regions in our study correspond to cloud cluster and clear regions in his. Despite the different methods of compositing and somewhat different areas and time periods considered, the two sets of results are remarkably similar, as evident from Fig. 2. It thus seems almost certain that the patterns obtained are real and not a consequence of observational error or of the approximations used in evaluating the budget. Both sets of results indicate that the apparent vorticity sources and sinks are largest in convectively active regions and that they act to reduce the vorticity changes being produced by the large-scale motions.

5. Results: Cloud mass flux and vorticity

The procedure described in Section 2 was applied next in order to determine the cloud mass flux and the in-cloud vorticity distribution. A fourth-order Runge-Kutta scheme was used in the computations. However, when applied to the foregoing data in the manner outlined, the procedure failed to yield zero mass flux near the tropopause for values of cloud base mass flux of a

TABLE 1. Vorticity balance in region of wave trough. Units: 10^{-11}sec^{-2}.

Level (mb)	$\frac{\partial\zeta}{\partial t}$	$U\frac{\partial\zeta}{\partial x}$	$\left(\beta\frac{\partial^2 U}{\partial y^2}\right)v$	$\omega\frac{\partial\zeta}{\partial p}$	$(\zeta+f)\nabla\cdot\mathbf{V}$	Residual or apparent vorticity source, Z
Sfc	1.1	0.2	1.6	0.0	−12.5	−10.0
900	−0.3	0.1	1.4	0.6	−10.0	− 8.2
800	−2.0	0.8	0.5	−1.0	− 8.7	−10.4
700	−1.4	0.7	−0.5	−2.8	− 1.8	− 5.8
600	0.1	0.0	−0.5	−3.2	− 1.7	− 5.3
500	−0.5	0.3	−0.2	−2.9	− 2.2	− 5.5
400	−1.4	1.0	−0.1	−1.8	− 0.5	− 2.8
300	−0.1	0.1	−2.1	−3.4	0.9	− 4.6
250	−2.2	1.8	−0.5	−4.4	7.0	1.7
200	−4.1	3.4	2.1	−1.2	12.8	13.0
175	−6.4	5.5	2.5	2.6	14.4	18.6
150	−5.2	4.4	2.5	3.3	14.1	19.1
125	−2.6	2.1	1.4	1.8	10.9	13.6
100	0.1	−0.1	0.0	0.0	3.6	3.6

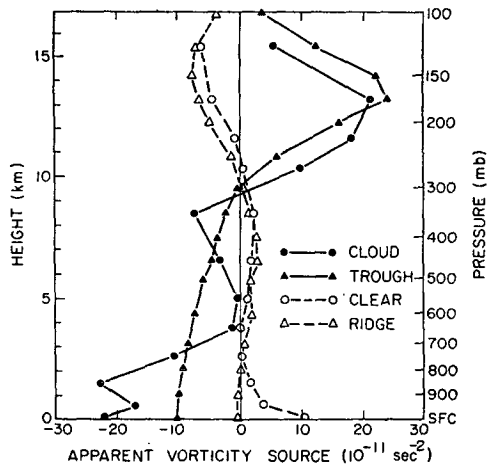

FIG. 2. Vertical profiles of the apparent vorticity source in trough and ridge regions of this study (triangles) and in cloud and clear regions of Williams's (1970) study (circles).

size generally considered reasonable from studies based on other methods. This shortcoming can be attributed to either of two causes: a deficiency in the physical formulation or uncertainties in the data. We have proceeded on the assumption that the latter is the cause and have searched for parameters which, if altered in an acceptable way, would lead to a more satisfactory solution. Further attention will be focused only on the region near the wave trough where the convective activity is greatest. In this region two such parameters were identified: the Z values in upper troposphere which if larger (more positive) would reduce the mass flux near the tropopause, and the cloud base vorticity which if smaller would have the same effect. We will now present arguments for altering these parameters in the desired senses.

In the case of the first of these parameters, it is noted from (14) below, an integrated form of the vorticity equation, that the mass-integrated Z values should equal the curl of the surface stress. Thus,

$$\frac{1}{g}\int_{p_T}^{p_0} Z\,dp = -\left(\frac{\partial\tau_{zy}}{\partial x}-\frac{\partial\tau_{zx}}{\partial y}\right)_0$$

$$= -\left[\frac{\partial}{\partial x}(\rho C_D|\bar{\mathbf{V}}|\bar{v}|)-\frac{\partial}{\partial y}(\rho C_D|\bar{\mathbf{V}}|\bar{u})\right]_0. \quad (14)$$

Here τ_{zy} and τ_{zx} are the northward and eastward components of the eddy stress on a horizontal surface, ρ is the density, C_D the drag coefficient, and u and v velocity components in the x and y directions. The subscripts 0 and T refer to the surface and tropopause values, respectively. It is assumed in (14) that the eddy stress is negligible at the tropopause. Measurement of the two sides of the equation reveals, however, a substantial difference between the integrated Z values and the curl of the surface stress as determined from the aero-

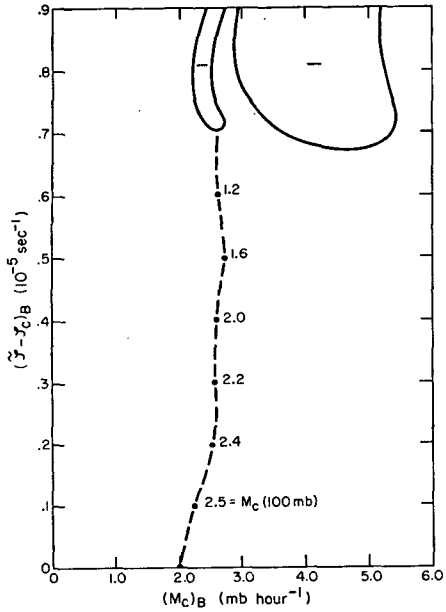

FIG. 3. Vertical cloud mass flux at 100 mb as a function of cloud base mass flux and difference between environmental and cloud vorticities at cloud base. The solid line indicates zero flux. Downward flux occurs in negative regions. See text for further explanation.

dynamic method when applied to twice-daily surface wind observations for the three-month period at the triangle of stations. With C_D computed from

$$C_D = (1.10 + 0.04V) \times 10^{-3},$$

where V is wind speed (m sec^{-1}), a value of -5.5×10^{-8} kg m^{-2} sec^{-2} is obtained for the curl of the surface stress as compared with a mass-integrated Z value of -25.6×10^{-8} kg m^{-2} sec^{-2}. A possible cause for the greater size of the latter is the compositing technique. The method uses the mean meridional wind component in the lower troposphere to define the wave sectors. If the vertical structure of the disturbances which comprise the composite wave varies somewhat from case to case, upper-level features tend to become blurred. Thus, the negative Z values at lower levels in the convective region can outweigh the positive values aloft by an amount in excess of that necessary to balance the surface frictional torque, as indeed was found. In view of the foregoing considerations the Z values above 300 mb were multiplied by a factor of 2.1 in further computations. This is the factor required to bring (14) into balance. It should be pointed out that the adjustment of the Z-values is required to make our data internally consistent irrespective of the type of cloud model employed.

As concerns the second parameter, the cloud base vorticity, we note that in the initial computations it was obtained from the vorticity balance in the subcloud layer and that its value was found to be quite sensitive to small changes in the quantities involved. We thus regard the estimated vorticity to be uncertain and inquire how the 100-mb mass flux is changed when its value is altered. The answer to this query is shown in Fig. 3 for a large range of assumed cloud base mass fluxes. The computations are based on (9) and (12) and make use of the adjusted Z values. The solid lines on the figure indicate combinations of cloud base mass flux and cloud base vorticity deficit for which the cloud mass flux goes to zero at 100 mb. For combinations with the negatively marked regions, downward flux is obtained at 100 mb. All other combinations give a remaining upward flux. The dashed line indicates, for a particular value of the cloud base vorticity deficit, the cloud base mass flux for which the mass flux at 100 mb is a minimum. The values of these minimum fluxes are labelled at intervals along the line.

From the figure we conclude that the cloud mass flux will vanish at high levels for cloud base fluxes in the range of 2–5 mb hr^{-1} provided the vorticity at cloud base is well below the environmental value. However, the required relative vorticity of about zero is an unacceptably small value. Thus in the final solution we have made an arbitrary but conservative choice for the cloud base vorticity, namely, the average value in the subcloud layer. This value is 0.6×10^{-5} sec^{-1}, or 0.1×10^{-5} sec^{-1} less than the ambient value, and is intermediate in size between that obtained from the subcloud-layer vorticity balance and from the condition of zero mass flux at 100 mb. From Fig. 3 it is seen that for this value of vorticity deficit, a cloud base mass flux of 2.2 mb hr^{-1} yields the minimum flux at 100 mb. We therefore regard this as the optimum choice for the lower boundary value and use it in (9) and (12), with the adjusted Z values and assumed cloud base vorticity, to obtain what we will regard as a best estimate of the vertical cloud mass flux and cloud vorticity distributions for the data and equations employed here. The results are shown in Figs. 4a and 4b.

The derived cloud mass flux distribution (solid line in Fig. 4a) resembles that for the mean mass flux (dashed line) except that the flux is larger at all levels. At the highest levels, the values are unreasonably excessive, as is to be expected from the previous discussion. The shape at lower levels differs from that obtained from the heat and moisture budgets by Yanai *et al.* (dot-dashed line) and by Reed and Johnson (dotted line). The vorticity budget yields an upward increase in flux whereas the other budgets result in a temporary decrease or near constancy of flux. It is difficult to assess the significance of the difference since the vorticity estimate is based on a single cloud type model and the others on a multiple cloud type. Possibly the vorticity results reflect mainly the contribution of the deep convection to the cloud mass flux (Cho and Ogura, 1974).

The cloud vorticity distribution (solid line in Fig. 4b) shows a maximum in-cloud vorticity at the 350-mb

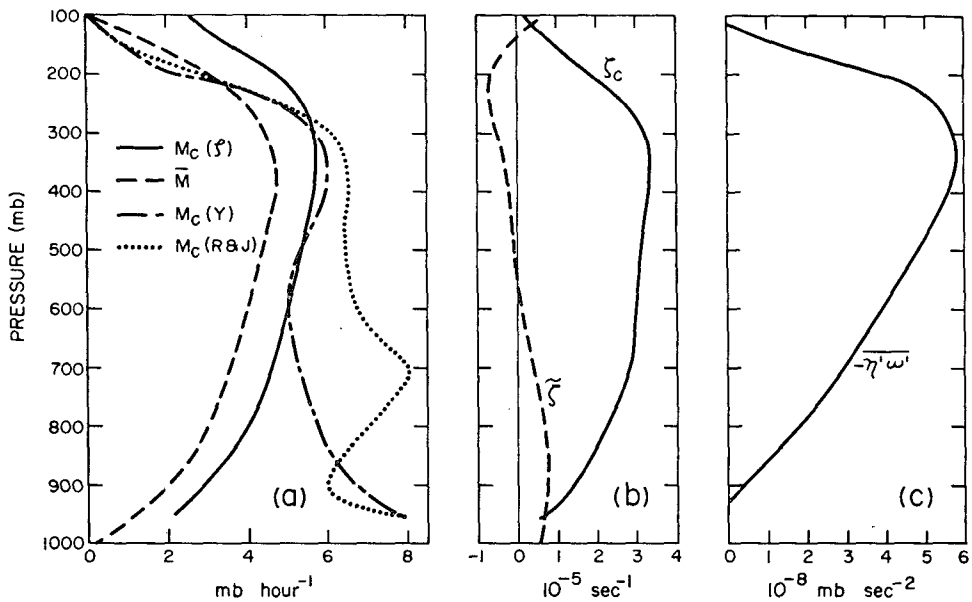

FIG. 4. (a) Vertical cloud mass flux: present study (solid line); according to Yanai *et al.* (dash-dotted line); according to Reed and Johnson (dotted line). Mean mass flux is given by dashed curve. (b) Profiles of environmental vorticity $\tilde{\zeta}$ and cloud vorticity ζ_c. (c) Profile of vertical eddy flux of vorticity.

level. Note that vorticities represented in this figure are relative vorticities ζ, and not absolute vorticities. The upward increase in vorticity must result from the horizontal convergence which the cloud mass undergoes at lower levels. Except near cloud base and top the cloud vorticity exceeds that in the environment (dashed line). The largest cloud vorticities observed, however, are still of approximately the same order of magnitude as the largest environmental values. Thus, it would be extremely difficult to verify the predicted values by direct measurement from airplane or other sensors capable of making observations on a small spatial scale.

6. Discussion

The foregoing observational results indicate that in the convectively active region of the tropical wave an apparent sink exists in the lower troposphere for the large-scale vorticity and an apparent source at high levels. The computations based on these results reveal that both the cloud mass flux and the in-cloud vorticity increase with height to the 350-mb level above which they diminish. Thus, since the vertical flux of vorticity,

$$-\overline{\eta'\omega'}=M_c(\eta_c-\tilde{\eta}), \tag{15}$$

is primarily determined by the M_c and η_c distributions, it too has its maximum at this level, as can be seen from Fig. 4c. The results shown in this figure are based on the adjusted Z values.

These findings suggest a simple physical explanation for the observed low-level vorticity sink and high-level source, namely, the removal of vorticity-rich air from low levels and its injection aloft by the convective-scale motions. This simple explanation is modified somewhat by the vorticity generation and depletion connected with the horizontal divergence fields within the clouds. By expanding (5) we see that

$$Z=\frac{\partial}{\partial p}[M_c(\eta_c-\tilde{\eta})]-\frac{\partial M_c}{\partial p}(\eta_c-\tilde{\eta}). \tag{16}$$

Thus, both the vertical flux divergence of vorticity and in-cloud horizontal divergence contribute to the observed Z field. Fig. 5 shows the separate terms and their

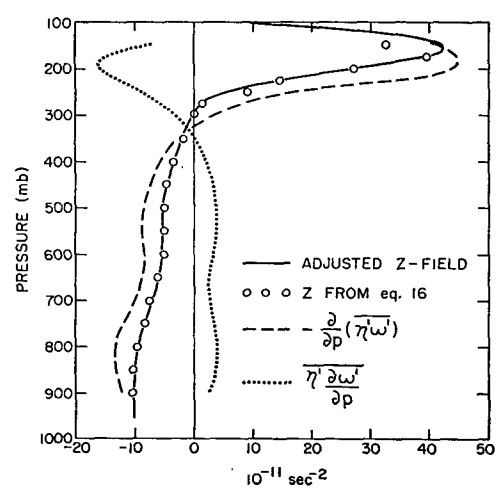

FIG. 5. Adjusted profile of apparent vorticity source (solid line), divergence of eddy vorticity flux (dashed), and eddy generation of vorticity by divergence effect (dotted). Open circles indicate sum of values of points on the latter two profiles.

sum (open circles) and also the adjusted Z field. The small discrepancies between the sum and the adjusted values arise from truncation errors in the finite-difference computations. The important point to note, however, is that it is the vertical flux divergence of vorticity which is primarily responsible for the apparent vorticity source and sink. The horizontal velocity divergence effect is smaller in magnitude and acts in the opposite sense. Consequently, to a first approximation, the simple explanation in terms of convective transport of vorticity holds.

7. Concluding remarks

In this paper we have confirmed earlier findings of large apparent vorticity sources and sinks in tropical disturbances, that is, of imbalances in the vorticity equation when applied to the large-scale variables. Our attempt to diagnose the cloud mass flux and cloud vorticity from this imbalance with use of a cloud ensemble model similar to that of Yanai *et al.* met with only limited success. A straightforward solution of the appropriate equations failed to yield a zero mass flux near the tropopause for any reasonable value of mass flux at the cloud base. We therefore sought an optimum solution, essentially by trial and error. This solution minimized the flux remaining at high levels while maintaining a physically plausible value for the vorticity at cloud base.

Despite the unsatisfactory nature of some of the procedures and results, the basic findings seem physically reasonable. Cloud mass flux, in-cloud vorticity, and vertical flux of vorticity all were found to reach maxima near 350 mb. Thus the observed lower tropospheric vorticity sink and the upper tropospheric source can be attributed to the removal of vorticity-rich air from low levels and its upward transport and deposition at high levels by the convection.

The mass flux profile at lower levels differed from that obtained in studies based on the large-scale heat and moisture budgets. The significance of the difference is not clear, however, since both methods involve numerous assumptions. The issue is not likely to be resolved until new and more definitive observational data become available. It is hoped that the GARP Atlantic Tropical Experiment (GATE) will provide the needed data.

Acknowledgments. The authors wish to thank E. E. Recker for his assistance in data processing, Dr. D. E. Colton for his contributions to the early phases of the study, and Prof. R. A. Houze, Jr., for reading the manuscript and offering suggestions. The research was supported by the National Science Foundation under Grant GA-32439.

REFERENCES

Cho, H.-R., and Y. Ogura, 1974: A relationship between the cloud activity and the low-level convergence as observed in Reed-Recker's composite easterly wave. *J. Atmos. Sci.*, **31** (in press).

Ogura, Y., and H.-R. Cho, 1973: Diagnostic determination of cumulus cloud populations from large-scale variables. *J. Atmos. Sci.*, **30**, 1276–1286.

Reed, R. J., and E. E. Recker, 1971: Structure and properties of synoptic-scale wave disturbances in the equatorial western Pacific. *J. Atmos. Sci.*, **28**, 1117–1133.

——, and R. H. Johnson, 1974: Diagnosis of cloud-population properties in tropical easterly waves. *Preprints Intern. Tropical Meteorology Meeting*, Vol. 2, Nairobi, Amer. Meteor. Soc.

Riehl, H., and R. P. Pearce, 1968: Studies on the interaction between synoptic and mesoscale weather elements in the tropics, Part II: Vorticity budgets derived from Caribbean data. Atmos. Sci. Paper No. 126, Colorado State University, 32 pp.

Wiederanders, C. J., 1961: Analyses of monthly mean resultant winds for standard pressure levels over the Pacific. Rept. No. 13, Hawaii Institute of Geophysics, University of Hawaii.

Williams, K. T., 1970: A statistical analysis of satellite-observed trade wind cloud clusters in the western North Pacific. Atmos. Sci. Paper No. 161, Colorado State University, 80 pp.

Yanai, Y., S. Esbensen and J.-H. Chu, 1973: Determination of bulk properties of tropical cloud clusters from large-scale heat and moisture budgets. *J. Atmos. Sci.*, **30**, 611–627.